Hindawi
International Journal of Forestry Research
Volume 2023, Article ID 5553957, 12 pages
https://doi.org/10.1155/2023/5553957

Research Article

Modeling and Mapping of Aboveground Biomass and Carbon Stock Using Sentinel-2 Imagery in Chure Region, Nepal

Ananta Poudel[1], **Him Lal Shrestha**[1], **Niraj Mahat**[2], **Garima Sharma**[1], **Sahara Aryal**[1], **Rupesh Kalakheti**[3] and **Basanta Lamsal**[3,4]

[1]*Kathmandu Forestry College, Tribhuvan University, Kathmandu, Nepal*
[2]*Institute of Forestry, Hetauda Campus, Tribhuvan University, Hetauda, Nepal*
[3]*Environmental Forum for Research and Development Nepal, Kathmandu, Nepal*
[4]*Department of International Relations and Diplomacy, Tribhuvan University, Kirtipur, Nepal*

Correspondence should be addressed to Ananta Poudel; apoudel816@gmail.com

Received 20 February 2023; Revised 11 May 2023; Accepted 12 May 2023; Published 19 May 2023

Academic Editor: Anna Źróbek-Sokolnik

The concerns about climate change in recent decades have heightened the need for effective methods for assessing and reporting forest biomass and Carbon Stocks (CS) at local, national, continental, and global scales. Accurate assessment of Aboveground Biomass (AGB) is critical for the sustainable management of forests, especially in the Chure region, a fragile and young mountainous in the lesser Himalaya of Nepal. This paper presents the modeling and mapping approach and shows how medium-resolution Sentinel-2 multispectral instrument (MSI) data can be used instead of hyperspectral data in inaccessible areas of the Chure region. The data were collected and analyzed from 72 circular sample plots. 60% (43 random sample plots) were used to create the model, while the remaining 40% (29 plots) were used for model validation. This study involved calculating 12 different vegetation indices and correlating them with plot-level AGB. Five models, including linear, logarithmic, quadratic, power, and exponential, were created, but the best model was found to be the quadratic model using normalized difference vegetation indices (NDVIs) with an R^2 value of 0.777 and a correlation coefficient of 0.881. The model's AIC and BIC values were 313.60 and 320.65, respectively. The validity of the model was performed using observed and predicted AGB values, resulting in an r value of 0.9128, an R^2 value of 0.8332, and an RMSE value of 10.7657 $t{\cdot}h^{-1}$. Finally, the developed regression equation was used to map AGB in the study area. The AGB per pixel ranges from 0 to 129.18 $t{\cdot}h^{-1}$, whereas the amount of CS ranges from 0 to 61.01 $t{\cdot}h^{-1}$. Among the different vegetation indices used in the study, NDVI was found to be more precise in estimating and mapping biomass and carbon stocks in this study. Therefore, the study recommends using the quadratic model of NDVI for accurate estimation of AGB and CS in the Chure region of Sainamaina municipality.

1. Introduction

Forests have a crucial function in reducing CO_2 levels in the atmosphere and the global climate system [1, 2]. Tropical forests, in particular, store a significant amount of carbon in biomass and soil, i.e., 56 and 32%, respectively [3]. However, they are being removed quickly, contributing to 12–20% of all human CO_2 emissions [4]. Recognizing this possibility, the United Nations Framework Convention on Climate Change (UNFCCC) established the reducing emission from deforestation and degradation and includes the role of conservation, sustainable management of forests, and enhancement of forest carbon stock (REDD+) scheme which incentivizes developing countries to conserve and manage their forests sustainably to reduce carbon emissions and promote sustainable development. For the mechanism to work, there must be transparent, comprehensive, steady, comparable, and precise national and subnational MRV (measurement, reporting, and verification) systems for forests to track and assess the amount of aboveground biomass/carbon stock and carbon emitted [5].

The aboveground biomass (AGB) is the most significant carbon pool in a tree; however, human activities such as deforestation can cause a reduction in forest area, resulting in deterioration of the AGB, carbon stock (CS), and CO_2 sequestration from the atmosphere. To track ecosystem responses to climate change and understand the global carbon cycle, forestry professionals, managers, and scientists need to perform terrestrial carbon accounting, which requires an assessment of AGB [6–9]. Therefore, to ensure accuracy, it is crucial to estimate biomass using a reliable method.

The two primary methods for estimating forest biomass are conventional field-based techniques and remote sensing (RS) methodologies. The conventional approach to estimating forest AGB is very precise [7] but laborious, expensive, and time-consuming [7, 10]. Combining RS and sample plot data to obtain spatially explicit estimates of forest AGB has become a common strategy [11]. RS techniques give an alternative to established methods of measuring biomass and CS [12]. The ability to estimate the spatial distribution of AGB at a reasonable cost with tolerable accuracy has led researchers to accept the use of RS in height [13] and in AGB estimation [7, 14, 15].

RS technologies have become a key tool for addressing some of the limitations associated with field data sampling by improving the accuracy of inventory estimates and lowering the costs of forest resource inventory and monitoring at landscape scales [16–18]. The majority of RS studies make use of optical (Landsat, Sentinel 2A, and LiDAR), synthetic aperture radar (SAR, Sentinel 1), or a combination of datasets for modeling and estimating AGB [11, 19–24]. Compared to techniques using radar and optical data, LiDAR systems have demonstrated a superior ability in forecasting and estimating AGB with greater precision [25]. However, its more extensive operational applications in estimating forest AGB in low- and middle-income countries with greater forest coverage are hindered by the data availability restrictions, high cost, and enormous data volume [26]. With the start of the European Union's Copernicus program, the global library of open access data has grown even more, with significant improvements in spatial, temporal, and radiometric precision [27, 28]. Sentinel-2 is a polar-orbiting sensor comprised of two satellites, each of which carries an MSI with a 290 km wide swath and a multipurpose design with 13 spectral bands spanning from visible and near-infrared (NIR) wavelengths to shortwave infrared wavelengths at fine (10, 20 m) and coarse (60 m) spatial resolution. The sensor has a high potential for mapping different vegetation characteristics due to the presence of four bands within the red-edge region, which are centered at 705 (band 5), 740 (band 6), 783 (band 7), and 865 nm (band 8a) [29]. Vegetation indices (VIs) are a mathematical combination of spectral bands computed by rationing, differencing, rationing differences, and sums by forming a linear combination of bands [30]. Many studies show that satellite-based VIs are most commonly employed for biomass modeling and estimation [21, 27, 31–33].

AGB was estimated in tropical forest of Mexico [34], Philippines [35], and India [36], using the Sentinel-2 imagery and random forest (RF), a machine learning algorithm to select the best model. Only a small number of AGB and CS estimation studies have been carried out in tropical forests with detailed ground-based quantification in Nepal despite the rapid advancements in RS. As per prior to our knowledge, Chure area lacks estimation of AGB and CS using combined efforts of RS and field ground data due to the complex topographical structure of Chure. Chure region is the youngest mountain range in the lesser Himalayas and is considered the most fragile and erodible [37]. It covers 12.8% of Nepal's land area and is home to 14% of the country's population [38]. The high population density in the Chure region has led to increased pressure on natural resources [39], which has resulted in deforestation and land degradation. Estimating AGB accurately is critical for quantifying the amount of carbon stored in forests, which is necessary for implementing REDD+ initiatives and establishing opportunities for carbon credit trading to promote forest conservation in the region. Few studies have been conducted in Nepal for estimating AGB with the integration of RS and field data. For example, Karna et al. [40] used WorldView-2 satellite images with small-footprint airborne LiDAR data to estimate tree carbon at the species level in a tropical forest in Nepal. Similarly, Baral Jamarkattel [41] achieved 61% accuracy when predicting the carbon content of a subtropical forest in central Nepal by integrating GeoEye and WorldView-2. A study by Koju et al. [19] used a two-scale approach for estimating AGB with optical RS images in a subtropical forest of Nepal. Kandel [20] estimates AGB and CS by integrating LiDAR, satellite images, and field measurement. Pandit et al. [21] estimate the AGB in subtropical buffer zone community forests using Sentinel 2 data. Qazi et al. [42] compare forest AGB estimates from passive and active RS sensors over Kayar Khola watershed. Similarly, Pandit et al. [43] perform AGB estimation in the buffer zone community forest of central Nepal coupling in situ measurement with Landsat 8 satellite data. Assessment of AGB and CS in Nepal is primarily focused on the subtropical and central parts of the Nepal.

The absence of baseline data on forest resources from the local to the regional level is one of the main obstacles to accurate forest AGB estimation in Nepal. This is still one of the major problems where the forest staff's ability to conduct an inventory is very limited. The cause could be attributed to a lack of technical assistance and excessive reliance on conventional field data collection techniques. To the best of our knowledge, this is the inaugural attempt to conduct a research study in the tropical forest of the Chure area and integrate Sentinel-2 spectrally derived indices with plot-level AGB to model and estimate AGB in Sainamaina municipality forest using modeling techniques.

2. Materials and Methods

2.1. Study Area. This study was conducted in the Chure area of Sainamaina municipality situated in the Rupandehi district of Nepal's Lumbini province. The geographical location of the study area is 83°15′44″E to 83°21′01″E longitude and 27°38′48″N to 27°46′05″N latitude Figure 1. The

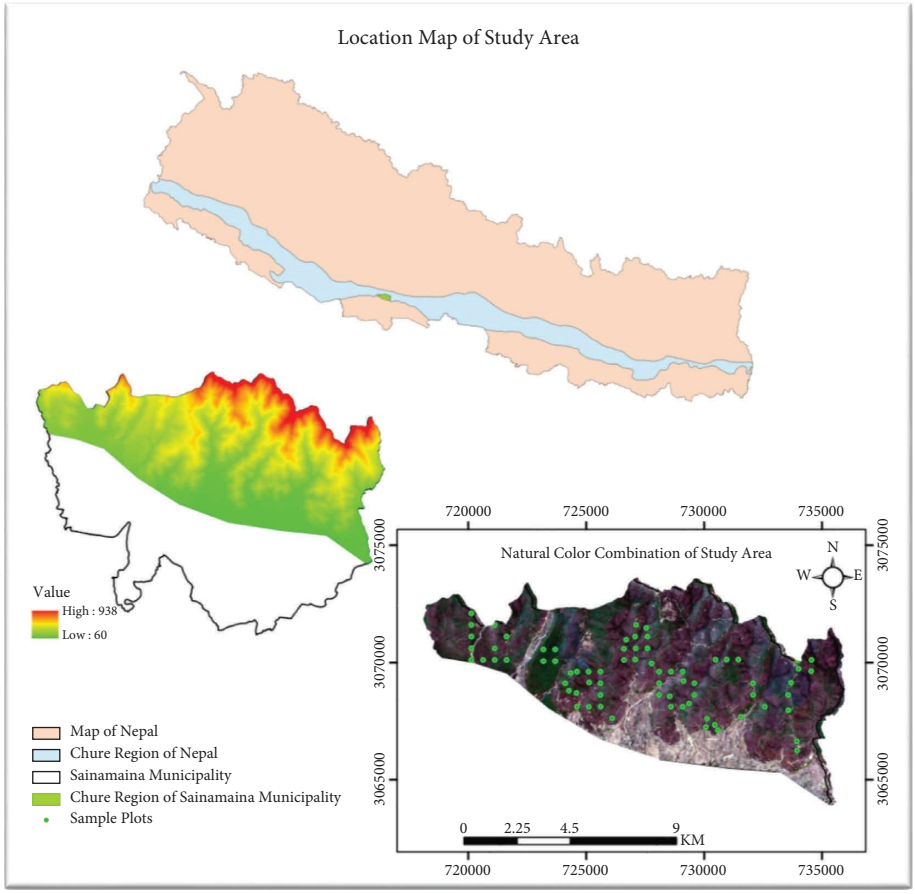

Figure 1: Map of the study area.

area of Chure region of Sainamaina municipality is 9235.11 ha [44]. The study area has typical tropical forest characteristics of undulating topography. Major species of this region are *Shorea robusta*, *Syzygium cumini*, *Lagerstroemia parviflora*, *Mallotus philippinensis*, and *Anogeissus latifolia*. The research site has a varied topography, with slopes ranging from 00 to 65.740 with an elevation ranging from 60 meter above sea level to 938 meters. The average annual precipitation in the area is 2600 mm, with 80% of the rainfall occurring during the monsoon season. In addition, the mean maximum and minimum temperatures recorded were 42.5°C and 7.5°C, respectively [45].

2.2. Data Collection

2.2.1. Sampling Strategy and Field Data Collection. To collect the data on vegetation in the study area, the grid of $2 * 2$ km was laid using ArcGIS. Each selected grid was chosen to represent the vegetation of the entire study area, as illustrated in Figure 2. Field data were collected between August and September 2021 using a circular sample plot of 500 m^2 (12.62-meter radius). A total of 72 plots (calculated by using the equation provided by the Community Forestry Inventory Guideline 2004) were sampled using a stratified random sampling method in ArcGIS 10.5. In some instances, sample plots were relocated to new coordinates up to 50 meters away due to inaccessibility. In each plot height, the diameter of an individual tree was measured at the breast height (DBH) of 1.3 meter above the ground level, and the species with DBH ≥ 8 cm were measured [46, 47]. Each tree species name was recorded in each plots.

2.2.2. Sentinel-2 Image Acquisition and Processing. The satellite image of Sentinel-2 level 1C was downloaded from the website of the European Space Agency (ESA) (https://sentinel.esa.int/web/sentinel/sentinel-data-access), which is composed of $100 * 100$ km^2 tiles dated 20th April 2021 for the study areas with $10\,m * 10\,m$ spatial resolution and the cloud cover less than 1%. The data are collected at 10, 20, and 60-meter spatial resolution in 13 spectral bands that span the visible, near-infrared (NIR), red-edge, and shortwave infrared (SWIR) wavelength ranges and had been previously preprocessed to reflect the top of the atmosphere (TOA). Sentinel-2 level 1C was processed to level 2A to gain the bottom of the atmosphere (BOA) corrected reflectance image using the ATCOR algorithm through Sen2Cor plugin in Sentinel Application Platform (SNAP) software. As the image had a spatial resolution of 10 m, it was considered adequate for the study. To ensure consistency, the image was resampled in SNAP to a spatial resolution of 10 m using the "Band 2" tile as the reference

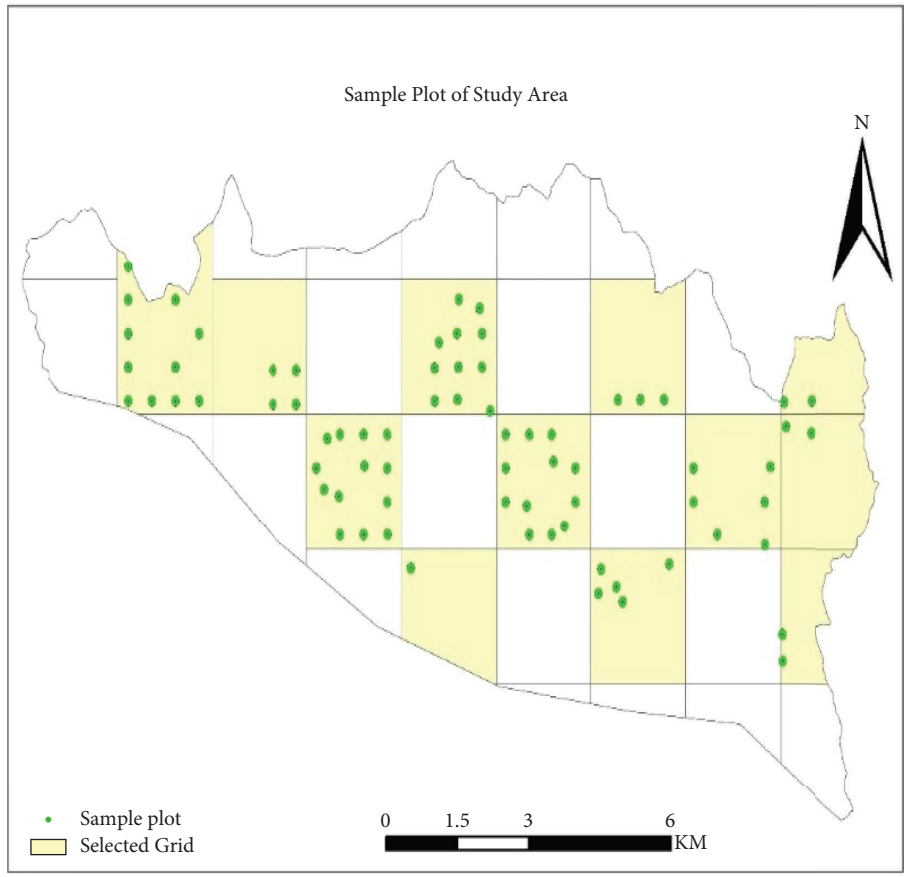

Figure 2: Grid selection and sample plots.

band source product. Finally, the image was subset to capture the research area in ArcMap.

2.3. Data Analysis

2.3.1. Field Data Analysis of AGB and CS. For this study, a revised and improved allometric equation adopted by Chave et al. [48] especially for tropical forest trees was used for estimating AGB. The equation by Chave et al. [48] is based on the diameter, height, and specific density of wood (ρ) for the calculation of AGB. Data on diameter and height were directly collected from the field, while specific wood density is derived from various literature reviews. Species with their default (ρ) values given by Khanna and Chaturvedi [49] and Thakur [50] was used to calculate tree level biomass. In the absence of specific values, a general value ($\rho = 0.674$) was used [21]. Individual biomass was calculated and then aggregated to obtain individual plot-level AGB:

$$AGB_{est} = 0.0673 * \left(\rho * D^2 * H\right)^{0.976}, \quad (1)$$

where AGB_{est} is AGB estimated in kilogram, D is DBH in cm, H is height in meter, ρ is wood density in g/cm^3, and 0.0673 and 0.976 are constants. Total AGB for individual plots was computed using equation (1) and then converted to ton per hectare (t·h^{-1}). Subsequently, the amount of CS was calculated from the AGB using the conversion factor (CF) of 0.47 [51]. CS was calculated using the following equation:

$$CS = AGB * CF, \quad (2)$$

where CS is the carbon stock in ton, AGB is the aboveground biomass, and CF is the carbon fraction (0.47).

2.3.2. Deriving VIs from the Sentinel-2 Optical Satellite Image. The Sentinel toolbox and the Raster calculator tool in ArcMap software were used to calculate a variety of vegetation indices (VIs) from the spectral bandwidths of the Sentinel-2 image. The selection of the specific VIs was based on their efficacy in previous studies focused on estimating biomass. There are over 150 different VIs available, but only 12 of them were chosen for this particular study based on their performances for analyzing and predicting the AGB. Table 1 provides the formulas and authors of the 12 selected indices.

2.3.3. Extraction of Pixel Values. The center of the sample plot location (latitude and longitude) was exported to a 12.62-meter circular plot using a buffer tool. The pixel values for all VIs were extracted using zonal statistics with the buffered circular plot location and exported in csv format for further analysis. Zonal statistics provide the average pixel value for the 12.62-meter plot by calculating the nearest

Table 1: VIs formula and their authors.

S. nos.	Formula of VIs	Authors
1	$NDVI = \rho NIR - \rho RED/\rho NIR + \rho RED$	Gitelson and Merzlyak [52]
2	$SR = \rho NIR/\rho RED$	Jordan [53]
3	$NDI45 = \rho RED1 - \rho RED/\rho RED1 + \rho RED$	Delegido et al. [54]
4	$S2REP = 700 + 35 \times (\rho RED3 + \rho RED/2) - \rho RED1/\rho RED2 - \rho RED1$	Frampton et al. [55]
5	$SIPI = \rho NIR - \rho B1/\rho NIR - \rho RED$	Penūelas et al. [56]
6	$SAVI = 1.5 \times \rho NIR - \rho RED/\rho NIR + \rho RED + 0.5$	Huete [57]
7	$NDWI = \rho G - \rho NIR/\rho G + \rho NIR$	McFeeters [58]
8	$RENDVI705 = \rho NIR - \rho RED1/\rho NIR + \rho RED1$	Puletti et al. [59]
9	$ARVI = \rho NIR - \rho RED - (\rho RED - \rho BLUE)/\rho NIR + \rho RED + (\rho RED - \rho BLUE)$	Kaufman and Tanre [60]
10	$RENDVI783 = \rho NIR - \rho RED3/\rho NIR + \rho RED3$	Huete et al. [61]
11	$EVI = 2.5 \times \rho NIR - \rho RED/1 + \rho NIR + 6 \times \rho RED - 7.5 \times \rho BLUE$	Huete et al. [62]
12	$EVI2 = 2.5 \times \rho NIR - \rho RED/\rho NIR + 2.4 \times \rho RED + 1$	Jiang et al. [63]

SR: simple ratio; NDI45: normalized difference index 45; S2REP: Sentinel-2 red edge position; SIPI: structure intensive pigment ratio; SAVI: soil-adjusted vegetation index; NDWI: normalized difference water index; RENDVI 705, 783: red-edge normalized difference vegetation index 705, 783; ARVI: atmospherically resistant vegetation index; EVI 2: enhanced vegetation index-2; NIR: near infrared, G: green.

neighbor pixel values if the area of the sample plot lies in multiple pixels.

2.4. Statistical Analysis. Statistical Package for Social Science (SPSS) and Microsoft Excel were used for statistical analysis. The relationship between each VI and AGB was assessed using five different functions, i.e., linear, logarithmic, quadratic, power, and exponential regression models. The general forms of five functions are given as equations (3)–(7). For all the abovementioned functions, AGB was used as a dependent variable (y) and VI was used as an independent variable (x) to determine change in AGB as change in VI. A total of 43 sample plots were used for analyzing the relation and model development, and 29 were used for model validation:

$$Y = \beta_0 + \beta_1 \times \mathrm{VI}, \tag{3}$$

$$Y = \beta_0 + \beta_1 \times \ln(\mathrm{VI}), \tag{4}$$

$$Y = \beta_0 + \beta_1 \times \mathrm{VI} + \beta_2 \times (\mathrm{VI})^2, \tag{5}$$

$$Y = \beta_0 \times (\mathrm{VI})^{\beta_1}, \tag{6}$$

$$Y = \beta_0 \times e^{\mathrm{VI} \times \beta_1}, \tag{7}$$

where Y is the aboveground biomass ($t{\cdot}h^{-1}$), VI is the value of vegetation indices, and β_0, β_1, and β_2 are parameters.

2.4.1. Model Performance Assessment. For assessing the model performance, a statistical evaluator was used, i.e., R^2. Generally, a higher R^2 value indicates the better performance of the model [64]. For this, the study model is built up with comparing AGB $t{\cdot}h^{-1}$ with different 12 VIs along 5 different regression models, and the model with an R^2 value higher than 0.70 was further selected to determine its consistency. To compare the best selected model of AGB with VIs, Adj. R^2 (8), RMSE, Akaike information criterion (AIC) (9), and Bayesian information criterion (BIC) (10) were used [64]. These criteria provide a simple and effective method for selecting and comparing regression models. The model with a high value of R^2_{adj} and a low value of RMSE, AIC, and BIC was considered to be the best for AGB estimators [65]:

$$R^2_{\mathrm{adj}} = 1 - \left(1 - \mathrm{R}^2\right) \frac{(\mathrm{N} - 1)}{(\mathrm{N} - \mathrm{p} - 1)}, \tag{8}$$

where N = number of samples, p = number of predictor value, and R^2 is the coefficient of determination:

$$\mathrm{AIC} = n \times \log \frac{\mathrm{SSE}}{n} + 2k, \tag{9}$$

$$\mathrm{BIC} = n \times \log \frac{\mathrm{SSE}}{n} + \log(n) \times k, \tag{10}$$

where n = number of plots, SEE = sum of squares due to errors, and k = number of parameters.

2.4.2. Model Validation. 29 sample plots were used for the model validations which are independent of the model development data. The predicted AGB obtained from the model was correlated with the calculated AGB to observe r and R^2 (11). Furthermore, the root mean square error (RMSE) (12) was also calculated:

$$R^2 = \frac{SQR}{SQT} = \frac{\sum_{i=1}^{n} \left(y_o - y_p\right)}{\sum_{i=1}^{n} \left(y_o - y_p\right)}, \tag{11}$$

$$\mathrm{RMSE} = \sqrt{\frac{\sum_{i=1}^{n} \left(y_o - y_p\right)^2}{n}}, \tag{12}$$

where n = number of sample plot (29), y_o is observed AGB, and y_p is the predicted AGB value for the plot i in $t{\cdot}h^{-1}$.

2.5. Mapping AGB and CS. The AGB and CS maps for the research area were estimated using a regression model constructed using VIs and AGB. After selection of the model and its validation, an AGB CS map of the entire research area was created in ArcGIS. The NDVI Raster map was selected in the algebra map expression in the Raster calculator, and

model equation (13) was applied. Every pixel value of NDVI is converted to biomass using the Raster calculator. Zero (0) values were allocated to no vegetation area. The amount of AGB and CS was further classified into five equal intervals.

3. Results

3.1. Common Species in the Chure Region of Sainamaina. Species identification and enumeration were also carried out in the field. A total of 929 trees were recorded from 72 sample plots. A total of 42 different species were recorded, and among them, the most occurring species were *Shorea robusta* (34.33%), *Bauchanania latifolia* (12.80%), *Terminalia alata* (10.87), *Anogeissus latifolia* (10.22%), *Lagerstroemia parviflora* (4.41%), *Semecarpus anacardium* (3.87%), *Acacia catechu* (2.47%), *Mallotus philippinensis* (2.36%), and *Syzygium cumini* (2.26%). The descriptive statistics for the forest parameter of 929 trees were recorded, i.e., height (m = meter) (min = 5, max = 28, average = 11.40 ± 0.15), DBH (cm = centimeter) (min = 8, max = 96, average = 24.20 ± 0.49), AGB ($t{\cdot}h^{-1}$) (min = 0.223, max = 172.90, average = 11.08 ± 0.68), and CS ($t{\cdot}h^{-1}$) (min = 0.11, max = 81.265, average = 5.174 ± 0.32)

3.2. Correlation Coefficient and Coefficient of Determination between VIs and AGB $t{\cdot}h^{-1}$. All of the vegetation indices (VIs) demonstrated a strong correlation with aboveground biomass (AGB) at the plot level, with all 12 VIs showing significance at a level of $p < 0.05$ at the 5% level of significance. A total of 60 models were evaluated (12 VIs ∗ 5 models) using plot-level biomass, and the indices with an R^2 value greater than 0.70 were selected as the best fit for the model. The overall R^2 value of all models has been summarized in Table 2.

3.3. Model Development and Validation. For the purpose of the model development, 43 sample plots were used and models with the value of $R^2 > 0.70$ were considered valid. Out of the 60 models tested, 18 were chosen for further analysis, with 10 being polynomial and 8 being linear models. The development of the models was based on criteria such as high R^2, high adjusted R^2 values, low RMSE, low AIC, and low BIC. The parameter estimates and fit statistics for each of the selected models are summarized in Table 3.

Analyzing Table 3, the quadratic form had a higher R^2 value than the linear form. This indicates that the quadratic model of NDVI, SAVI, and ARVI was able to explain approximately 78% of the variation in AGB per hectare, while the remaining 22% was explained by other variables that were not included in the model. Similarly, performance increased with the decrease in AIC and BIC values of variable NDVI (AIC = 313.60 and BIC = 320.65) than that of SAVI (AIC = 319.62 and BIC = 320.67) and ARVI (AIC = 313.78 and BIC = 320.85). All these 3 models show the values quite close to each other; thus, a model validation was performed using 29 sample plot data, and accuracy assessment was performed using the values of r, R^2, and RMSE. The scatterplot of the observed and estimated AGB was plotted for NDVI, ARVI, and SAVI as shown in Figure 3.

Table 4 presents the validation of the model based on the estimated and observed AGB for the quadratic model of NDVI, ARVI, and SAVI with the criterion value of r, R^2, and RMSE.

Analyzing the model validation result, the quadratic regression model of NDVI was selected as the best fit if the model was based on the value of r, R^2, and RMSE than that of SAVI and ARVI as shown in Table 4. The correlation between estimated and observed AGB gave a strong R^2 of 0.8332 and RMSE of 10.765 $t{\cdot}h^{-1}$. About 83% of the observed AGB was explained by the estimated AGB according to the quadratic model of NDVI. The general form of quadratic function as equation is as follows:

$$Y = \beta_0 + \beta_1 X + \beta_2 X^2, \quad (13)$$

where Y is the predicted biomass, β_0 is the y-intercept which is 26.676, and β_1 and β_2 are the slopes which are −125.73 and 304.0, respectively, and X is the NDVI:

$$Y = 26.676 - 125.73 * \text{NDVI} + 304.0 * (\text{NDVI})^2. \quad (14)$$

3.4. Mapping of AGB and CS. Figure 4 illustrates the prediction map resulted from quadratic regression models between NDVI and AGB. The result shows the AGB ranges mostly from 0 to 129.81 $t{\cdot}h^{-1}$. Subsequently, the CS map follows a similar pattern to the AGB map as the total amount of forest AGB was multiplied by 0.47 (47% of the AGB). Consequently, there is a higher amount of carbon content in those areas where AGB is higher. The amount of CS ranges mostly from 0 to 61.0 $t{\cdot}h^{-1}$

4. Discussion

For an intricate topographic structure, modeling and mapping forest AGB and CS are an extremely difficult task. For estimating AGB at the regional level, the application of freely accessible multispectral sensors could be a good substitute, especially in places where access to hyperspectral images is scarce. Therefore, we determine the model and map of the AGB and CS using Sentinel-2 (MSI) spectrally derived VIs with ground-based quantification of data using several regression modeling approaches in the Chure area of Sainamaina Municipality.

A positive correlation was observed between the VIs and AGB. Sentinel-2 derived VIs (S2REP and NDI45) show the minimum correlation as compared to other VIs. Among them, the quadratic model of NDVI, SAVI, ARVI, and RENDVI705 possess the maximum correlation and the coefficient of determination value. The result was addressed by Pandit et al. [21], where an R^2 value for SAVI, RENDVI705, S2REP, and NDVI was 0.81, 0.76, 0.75, and 0.70, respectively. The correlation value of 0.89 and 0.81 for the indices NDI45 and NDVI was obtained by Nuthammachot et al. [66] in private forest in Indonesia. Muhsoni

Table 2: R^2 between AGB and VIs (with 5 different models).

	VIs	R^2				
		Linear	Logarithmic	Quadratic	Power	Exponential
1	NDVI	**0.7333****	0.6808**	**0.7771****	0.6073**	0.6167**
2	SR	**0.7154****	0.6508**	**0.7193****	0.5766**	0.5728**
3	NDI45	0.6793**	0.6118**	**0.7095****	0.5263**	0.5453**
4	S2REP	0.4682**	0.4870**	0.6307**	0.5093**	0.4962**
5	SIPI	0.5729**	0.6143**	**0.7187****	0.5557**	0.5317**
6	SAVI	**0.7333****	0.6808**	**0.7771****	0.6073**	0.6167**
7	NDWI	0.5652**	0.5361**	0.6451**	0.4874**	0.5002**
8	RENDVI 705	**0.7159****	0.6284**	**0.7287****	0.5923**	0.6124**
9	ARVI	**0.7546****	0.6441**	**0.7787****	0.5976**	0.6203**
10	RENDVI 783	**0.7413****	0.6879**	**0.7739****	0.6219**	0.6307**
11	EVI	**0.7355****	0.6941**	**0.7359****	0.6099**	0.6011**
12	EVI2	**0.7490****	0.6914**	**0.7747****	0.6111**	0.6168**

**Significant at the 0.01 level (2-tailed). Values of R^2 greater than 0.70 has been highlighted (bold).

Table 3: Model development table with parameter estimates and fit statistics.

	Parameter estimates			Forms of equation	Fit statistics				
	β_0	β_1	β_2		R^2	RMSE	R^2 adj	AIC	BIC
NDVI	−23.18	131.73		Linear	0.73	9.25	0.73	319.33	324.61
NDVI	26.68	−125.73	304.00	Quadratic	0.78	8.45	0.77	313.60	320.65
SR	−4.73	17.28		Linear	0.72	9.55	0.71	322.12	327.41
SR	0.40	11.88	1.16	Quadratic	0.72	9.49	0.71	323.53	330.58
NDI45	12.84	−34.24	555.87	Quadratic	0.71	9.65	0.70	324.99	332.04
SIPI	392.68	−440.26	127.87	Quadratic	0.72	9.50	0.71	323.62	330.67
SAVI	−23.18	87.84		Linear	0.73	9.25	0.73	319.33	324.61
SAVI	26.67	−83.81	135.13	Quadratic	0.78	8.47	0.77	313.62	320.67
RENDVI705	−3.68	222.82		Linear	0.72	9.54	0.71	322.05	327.33
RENDVI705	6.22	74.65	445.59	Quadratic	0.73	9.33	0.72	322.05	329.10
ARVI	2.25	134.70		Linear	0.75	8.87	0.75	315.75	321.03
ARVI	10.75	32.79	217.45	Quadratic	0.78	8.47	0.77	313.78	320.85
RENDVI783	−26.34	234.78		Linear	0.74	9.11	0.74	318.01	323.29
RENDVI783	18.07	−145.14	749.52	Quadratic	0.77	8.51	0.76	314.22	321.26
EVI	−7.81	37.45		Linear	0.74	9.21	0.73	318.96	324.25
EVI	−5.73	33.13	1.87	Quadratic	0.74	9.20	0.72	320.90	327.94
EVI2	−14.53	60.99		Linear	0.75	8.97	0.74	316.71	321.99
EVI2	10.76	−11.75	45.92	Quadratic	0.77	8.50	0.76	314.07	321.12

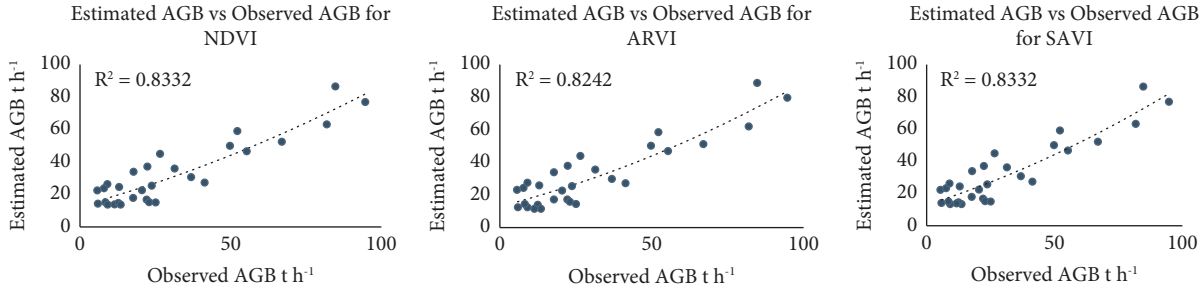

Figure 3: Scatterplot of estimated and observed AGB for the quadratic model of NDVI, ARVI, and SAVI.

Table 4: Validation of the model of different VIs.

Indices	Form of equation	R	R^2	RMSE
NDVI	Quadratic	0.9128	0.8332	10.7657
ARVI	Quadratic	0.90785	0.8242	10.8951
SAVI	Quadratic	0.91005	0.8282	10.7658

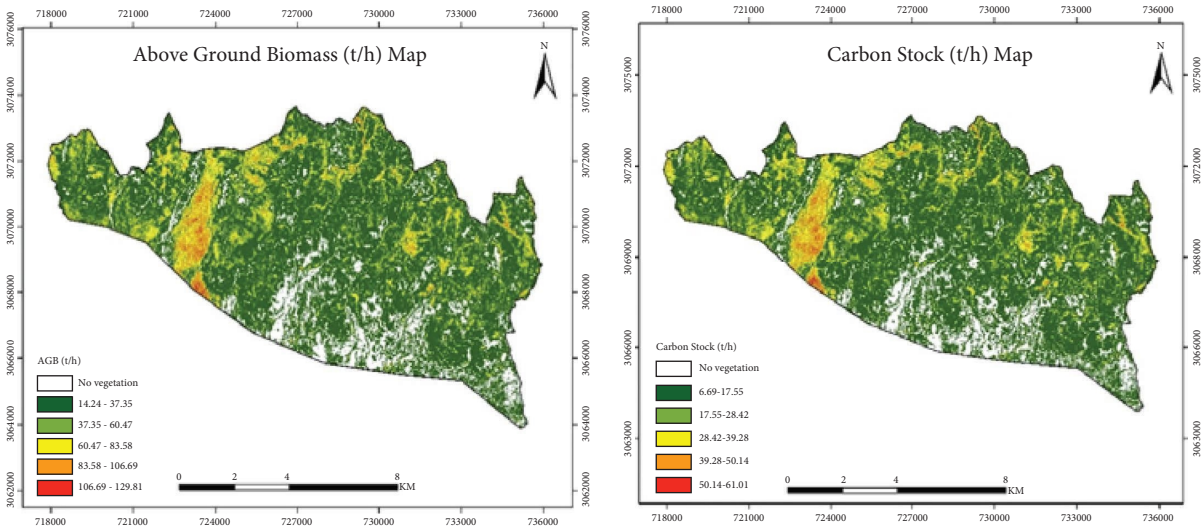

Figure 4: Map of AGB and CS developed from the model in t·h^{-1}.

et al. [67] obtained an R^2 value of 0.814 for the quadratic model while comparing 24 different VIs using Sentinel-2 for mangrove densities. Adan [68] in her study stated that an exponential model explains better than a linear model when combined with AGB and VI (RERVI) with $R^2 = 0.66$. Askar et al. [47] gained an R^2 value of NDI45, NDVI, and S2REP to be 0.79, 0.65, and 0.19, respectively, in private forest in Indonesia using Sentinel-2. Priatama et al. [69] calculated the correlation value of NDVI and SAVI to be 0.73 and 0.80 using Landsat imagery in a postmining area. NDI45 and S2REP have shown more values of r and R^2 than NDVI, and this might be due to the use red-edge region centered at 705 (band 5), 740 (band 6), 783 (band 7), and 865 nm (band 8a) in the formula as it provides the sensor a lot of potential for monitoring various vegetation features [29]. Furthermore, studies such as [47, 66, 70–72] have demonstrated that red-edge VIs diminish saturation, particularly in complex vegetation structures. Saturation occurs particularly when vegetation reaches maturity in the case of crops [73, 74], while in many cases, it is because of the complex forest structure [75–77] causing issues in predicting forest AGB [78]. In such a case, the VIs are unable to detect any further increases in biomass because saturation occurs when vegetation completely covers the land, which is frequently expressed as full leaf area coverage. In this case, the biomass continues to grow, while the indices remain unchanged. When compared to dense forests, VIs perform better in simple structure forests [79]. Similarly, Steininger [80] reported saturation at around 150 t·h^{-1}. This study concludes the average AGB from the field data to be 142.90 t·h^{-1}. Similarly, from the model, it is predicted that AGB for this study area to be between 14.24 and 129.81 t·h^{-1} which is lower than the saturation amount and that CS for the study area to be between 6.69 and 61.01 t·h^{-1}. Thus, the data saturation problem is eliminated in this study area due to lower canopy, and the AGB can be predicted using the VIs consisting of the NIR and red band, i.e., NDVI. This study predicted the quadratic model of NDVI as the best model for predicting the AGB and CS with an R^2 value of 83% between the observed and predicted and an RMSE value of 10.7657 t·h^{-1}. DFRS [81] calculated total AGB of live trees to be 179.00 t·h^{-1} (stem = 127.28, branch = 43.99, and foliage = 7.73 t·h^{-1}) and CS 84.73 t·h^{-1} (combined). The study includes only the stem of the live tree on estimating the AGB and CS based on the height and diameter of trees. The result from our predictive model is more likely similar with the study of Dfrs [81], and this might be due to as Dfrs collected from the many sample from the Chure area too.

Different studies used different models with different combination of RS to estimate the biomass of different types of forest. Sinha et al. [77] used a combination of ALOS PALSAR and Landsat TM to estimate tropical forest biomass. The NDVI calculated from optical image spectral bands had a poor relationship with biomass, with an R^2 of 0.29, which contradicts with the finding of our study which might be possibly due to saturation issues in the tropical forest. Similarly, Badreldin and Sanchez-Azofeifa [82] devised a method for integrating airborne LiDAR, TLS, and multitemporal Landsat satellite images in order to determine the relationship between forest stand parameters and VIs derived from Landsat optical satellite images. The study used stepwise multiple regression analysis, canopy height, and VIs to develop a best fit model for biomass estimation (NDVI, EVI2, and TCA). The best model had an R^2 of 0.78 and an RMSE of 44 Mg/hectare, and the value of R^2 aligns, while the RMSE contradicts with our study. This might be due to the use of stepwise multiple regression and use of more than one predictor variables. Macave et al. [83] used the regression model to relate AGB with different combinations of sensor data using RMSE, AIC, and BIC and from field data, and the mean AGB and CS were calculated to be 56 Mg·h^{-1} and 28 Mg·C·h^{-1}, respectively. For NSR, the best model projected AGB to be 63 ± 20.3 Mg·h^{-1}, with a range of 0.6 to 200 Mg·h^{-1} ($r^2 = 87.5$ percent, AIC = 123, and BIC = 51.93). The RMSE percent of the mean field estimate of 56 Mg·h^{-1} was found to be 20.46, the range of the AGB, AIC,

and BIC value does not align with our study, and as a matter of fact, Macave et al. [83] used the fusion of optical and radar data with the use of multiple regression. Likewise, Pandit et al. [21] produced an AGB map for subtropical buffer zone community forests of Nepal, where the best predictor variables from the final model generated by the RF algorithm were used. Sentinel-2 spectral bands and spectral-derived VIs were selected for biomass estimations with $R^2 = 0.81$ and RMSE = 25.22 t·h^{-1}. The RMSE does not align as our study is conducted in the tropical area; also, our study uses the parametric techniques, while Pandit uses the nonparametric algorithms as random forest (RF). Pandit et al. [43] tested two statistical approaches, namely, multiple linear regression (MLR) and RF, in estimating the AGB and concluded that the RF algorithm produced better results ($R^2 = 0.95$ and RMSE = 13.3 t·h^{-1}) than the MLR model ($R^2 = 0.56$ and RMSE = 37.01 t·h^{-1}).

The data analysis adopted in our method is solely based on the parametric test as it assumes the mathematical property of the data and provides an accuracy of 83.3% by the prediction model. However, the level of precision rises with the use of machine learning techniques. In recent years, machine learning techniques such as random forest (RF), support vector machines (SVMs), and artificial neural networks (ANNs) have become more popular in estimating forest AGB [84]. These machine learning methods are a more trustworthy approach to AGB estimation [85] as they do not have predetermined model structures, and the model structure is determined by the data. Ou et al. [86] compared two parametric models (linear regression model and linear regression with combined variables) with two nonparametric models (RF and ANN) and found that the latter resulted in significantly higher R^2 and RMSE for forest AGB estimation. Other studies have also supported this idea, suggesting that nonparametric models are better suited to capture the heterogeneity of forest AGB than parametric models [26, 87].

It is worth noting that previous RS research has yielded a variety of results for numerous modeling approaches to the empirical estimation of AGB employing RS and field data. It is difficult to determine the superiority of one method to other. Thus, each application necessitates an evaluation of the optical bands and indices to estimate biomass [7, 31], considering the forest type, topographical features, and study objectives. The future research should not be limited to the particular sensor or modeling approaches, it should get diversified by using various sensors as optical (Landsat, Sentinel 2A, and LiDAR) and synthetic aperture radar (SAR, Sentinel 1) with a combination of parametric (linear and multiple regression models) and nonparametric algorithms such as RF, SVM, ANN, multilayer perceptron artificial neural network (MLPNN), k-nearest neighbor (kNN), and support vector regression (SVR).

5. Conclusion

Here, we investigated the utility of Sentinel-2 VIs in estimating AGB and CS using five different regression model techniques in the Chure area of Sainamaina municipality. We concluded that the quadratic regression model of normalized difference vegetation indices shows the maximum value of the correlation coefficient and the coefficient of determination. Sentinel-2 data effectively predicted the AGB and CS of the study area with an R^2 value of 0.83 and an RMSE value of 10.7657 t·h^{-1}. Improvements in the spatial resolution (10 and 20 m) of Sentinel-2 MSI have the potential to enable satisfactory predictions of biomass in the Chure area of Sainamaina municipality.

Overall, our findings show the utility, potential, and power of combining in situ data with Sentinel-2 VIs in predicting biomass. The methodology here is relatively simple and applicable to other parts of Chure region sharing similar biophysical patterns and also where hyperspectral data are scarce. Sentinel-2 is a viable option for researchers and conservationists seeking low-cost, efficient, and freely available satellite sensor data for reliable and accurate monitoring of AGB and CS in areas where ground data are scarce. This study helps in the improved and sustainable forest management, climate change mitigation, biodiversity conservation, and land use planning. It can also be used in preparation of Sainamaina municipality forest and environment policy, climate change adaptation action plan, and sustainable development action plan as endorsed in Chapter 15, Section 102, Subsection 1 of Local Government Operation Act 2017 of Nepal.

Data Availability

The data presented in this study are available on request from the corresponding authors.

Conflicts of Interest

The authors declare that there are no conflicts of interest regarding the publication of this article.

Acknowledgments

The authors would like to thank Mr. Megh Bahadur Saru for his continuous help during the field data collection period. The authors would also like to thank subdivision forest officials for providing the information about the field study and for the selection of the grid. This study was funded by Agro-Forestry Promotion, Nepal.

References

[1] R. Alkama and A. Cescatti, "Biophysical climate impacts of recent changes in global forest cover," *Science*, vol. 351, no. 6273, pp. 600–604, 2016.

[2] Y. Pan, R. A. Birdsey, O. L. Phillips, and R. B. Jackson, "The structure, distribution, and biomass of the world's forests," *Annual Review of Ecology, Evolution and Systematics*, vol. 44, no. 1, pp. 593–622, 2013.

[3] Y. Pan, R. A. Birdsey, J. Fang et al., "A large and persistent carbon sink in the world's forests," *Science*, vol. 333, no. 6045, pp. 988–993, 2011.

[4] M. Collins, "Quantifying environmental indicators and assessing performance in tropical forest management," 2015.

[5] S. Mermoz, A. Bouvet, T. Le Toan, and R. Mathieu, "UNDER-estimation of biomass loss with REDD+ standard reporting method," in *Proceedings of the 2015 IEEE International Geoscience and Remote Sensing Symposium (IGARSS)*, pp. 3882–3885, IEEE, Milan, Italy, July 2015.

[6] İ. Güneralp, A. M. Filippi, and J. Randall, "Estimation of floodplain aboveground biomass using multispectral remote sensing and nonparametric modeling," *International Journal of Applied Earth Observation and Geoinformation*, vol. 33, pp. 119–126, 2014.

[7] D. Lu, "The potential and challenge of remote sensing-based biomass estimation," *International Journal of Remote Sensing*, vol. 27, no. 7, pp. 1297–1328, 2006.

[8] T. S. Chinembiri, M. C. Bronsveld, D. G. Rossiter, and T. Dube, "The precision of C stock estimation in the Ludhikola watershed using model-based and design-based approaches," *Natural Resources Research*, vol. 22, no. 4, pp. 297–309, 2013.

[9] T. W. Gara, A. Murwira, E. Chivhenge, T. Dube, and T. Bangira, "Estimating wood volume from canopy area in deciduous woodlands of Zimbabwe," *Southern Forests: A Journal of Forest Science*, vol. 76, no. 4, pp. 237–244, 2014.

[10] M. Henry, N. Picard, C. Trotta et al., "Estimating tree biomass of sub-Saharan African forests: a review of available allometric equations," *Silva Fennica*, vol. 45, no. 3B, pp. 477–569, 2011.

[11] A. C. Vibrans, R. E. McRoberts, P. Moser, and A. L. Nicoletti, "Using satellite image-based maps and ground inventory data to estimate the area of the remaining Atlantic forest in the Brazilian state of Santa Catarina," *Remote Sensing of Environment*, vol. 130, pp. 87–95, 2013.

[12] F. Rosillo-Calle and J. Woods, *The Biomass Assessment Handbook*, Routledge, England, UK, 2012.

[13] K. Tiwari and L. L. Narine, "A comparison of machine learning and geostatistical approaches for mapping forest canopy height over the southeastern US using ICESat-2," *Remote Sensing*, vol. 14, no. 22, p. 5651, 2022.

[14] R. DeFries, F. Achard, S. Brown et al., "Earth observations for estimating greenhouse gas emissions from deforestation in developing countries," *Environmental Science & Policy*, vol. 10, no. 4, pp. 385–394, 2007.

[15] M. S. R. Murthy, S. Wesselman, and H. Gilani, "Multi-scale forest biomass assessment and monitoring in the Hindu Kush Himalayan region: a geospatial perspective," *International Centre for Integrated Mountain Development (ICIMOD)*, vol. 34, 2015.

[16] E. Naesset, H. O. Ørka, S. Solberg et al., "Mapping and estimating forest area and aboveground biomass in miombo woodlands in Tanzania using data from airborne laser scanning, TanDEM-X, RapidEye, and global forest maps: a comparison of estimated precision," *Remote Sensing of Environment*, vol. 175, pp. 282–300, 2016.

[17] R. E. McRoberts, E. Næsset, and T. Gobakken, "Estimation for inaccessible and non-sampled forest areas using model-based inference and remotely sensed auxiliary information," *Remote Sensing of Environment*, vol. 154, pp. 226–233, 2014.

[18] J. Esteban, R. E. McRoberts, A. Fernández-Landa, J. L. Tomé, and M. Marchamalo, "A model-based volume estimator that accounts for both land cover misclassification and model prediction uncertainty," *Remote Sensing*, vol. 12, no. 20, p. 3360, 2020.

[19] U. A. Koju, J. Zhang, S. Maharjan et al., "A two-scale approach for estimating forest aboveground biomass with optical remote sensing images in a subtropical forest of Nepal," *Journal of Research*, vol. 30, no. 6, pp. 2119–2136, 2019.

[20] P. N. Kandel, "Estimation of above ground forest biomass and carbon stock by integrating LiDAR, satellite image and field measurement in Nepal," *Journal of Natural History Museum*, vol. 28, pp. 160–170, 2015.

[21] S. Pandit, S. Tsuyuki, and T. Dube, "Estimating above-ground biomass in sub-tropical buffer zone community forests, Nepal, using Sentinel 2 data," *Remote Sensing*, vol. 10, no. 4, p. 601, 2018.

[22] E. H. Hansen, T. Gobakken, O. M. Bollandsås, E. Zahabu, and E. Næsset, "Modeling aboveground biomass in dense tropical submontane rainforest using airborne laser scanner data," *Remote Sensing*, vol. 7, no. 1, pp. 788–807, 2015.

[23] S. S. Saatchi, N. L. Harris, S. Brown et al., "Benchmark map of forest carbon stocks in tropical regions across three continents," *Proceedings of the National Academy of Sciences*, vol. 108, no. 24, pp. 9899–9904, 2011.

[24] N. L. Harris, S. Brown, S. C. Hagen et al., "Baseline map of carbon emissions from deforestation in tropical regions," *Science*, vol. 336, no. 6088, pp. 1573–1576, 82012.

[25] S. Tian, M. A. Tanase, R. Panciera, J. Hacker, and K. Lowell, "Forest biomass estimation using radar and LiDAR synergies," in *Proceedings of the 2013 IEEE International Geoscience and Remote Sensing Symposium - IGARSS*, pp. 2145–2148, IEEE, Melbourne, VIC, Australia, July 2013.

[26] P. Zhao, D. Lu, G. Wang et al., "Forest aboveground biomass estimation in Zhejiang Province using the integration of Landsat TM and ALOS PALSAR data," *International Journal of Applied Earth Observation and Geoinformation*, vol. 53, pp. 1–15, 2016.

[27] C. Li, L. Zhou, and W. Xu, "Estimating aboveground biomass using Sentinel-2 MSI data and ensemble algorithms for grassland in the Shengjin Lake Wetland, China," *Remote Sensing*, vol. 13, no. 8, p. 1595, 2021.

[28] H. Astola, T. Häme, L. Sirro, M. Molinier, and J. Kilpi, "Comparison of Sentinel-2 and Landsat 8 imagery for forest variable prediction in boreal region," *Remote Sensing of Environment*, vol. 223, pp. 257–273, 2019.

[29] C. Shoko and O. Mutanga, "Examining the strength of the newly-launched Sentinel 2 MSI sensor in detecting and discriminating subtle differences between C3 and C4 grass species," *ISPRS Journal of Photogrammetry and Remote Sensing*, vol. 129, pp. 32–40, 2017.

[30] J. Hanes, *Biophysical Applications of Satellite Remote Sensing*, Springer Science & Business Media, Berlin, Germany, 2013.

[31] G. M. Foody, D. S. Boyd, and M. E. J. Cutler, "Predictive relations of tropical forest biomass from Landsat TM data and their transferability between regions," *Remote Sensing of Environment*, vol. 85, no. 4, pp. 463–474, 2003.

[32] P. Lourenço, "Biomass estimation using satellite-based data," *For Biomass - From Trees to Energy*, 2021.

[33] D. Utari, M. Kamal, and F. Sidik, "Above-ground biomass estimation of mangrove forest using WorldView-2 imagery in Perancak Estuary, Bali," *IOP Conference Series: Earth and Environmental Science*, vol. 500, p. 12011, 2020.

[34] J. L. Hernández-Stefanoni, M. Á. Castillo-Santiago, J. F. Mas et al., "Improving aboveground biomass maps of tropical dry forests by integrating LiDAR, ALOS PALSAR, climate and field data," *Carbon Balance and Management*, vol. 15, pp. 15–17, 2020.

[35] J. A. A. Castillo, A. A. Apan, T. N. Maraseni, and S. G. Salmo, "Estimation and mapping of above-ground biomass of mangrove forests and their replacement land uses in the Philippines using Sentinel imagery," *ISPRS Journal of Photogrammetry and Remote Sensing*, vol. 134, pp. 70–85, 2017.

[36] S. M. Ghosh and M. D. Behera, "Aboveground biomass estimation using multi-sensor data synergy and machine learning algorithms in a dense tropical forest," *Applied Geography*, vol. 96, pp. 29–40, 2018.
[37] G. N. Chure, "Terai madhesh conservation or management master plan," 2018.
[38] D. Bishwokarma, S. J. Thing, and N. S. Paudel, "Political ecology of the Chure region in Nepal," *Journal of Forest and Livelihood*, vol. 14, no. 1, pp. 84–96, 2019.
[39] B. K. Singh, "Land tenure and conservation in Chure," *Journal of Forest and Livelihood*, vol. 15, no. 1, pp. 87–102, 2017.
[40] Y. K. Karna, Y. A. Hussin, H. Gilani et al., "Integration of WorldView-2 and airborne LiDAR data for tree species level carbon stock mapping in Kayar Khola watershed, Nepal," *International Journal of Applied Earth Observation and Geoinformation*, vol. 38, pp. 280–291, 2015.
[41] S. Baral Jamarkattel, *Mapping Carbon Stock Using High Resolution Satellite Images in Sub-tropical forest of Nepal*, University of Twente, Enschede, Netherlands, 2011.
[42] W. A. Qazi, S. Baig, H. Gilani, M. M. Waqar, A. Dhakal, and A. Ammar, "Comparison of forest aboveground biomass estimates from passive and active remote sensing sensors over Kayar Khola watershed, Chitwan district, Nepal," *Journal of Applied Remote Sensing*, vol. 11, no. 2, p. 26038, 2017.
[43] S. Pandit, S. Tsuyuki, and T. Dube, "Landscape-scale aboveground biomass estimation in buffer zone community forests of Central Nepal: coupling in situ measurements with Landsat 8 Satellite Data," *Remote Sensing*, vol. 10, no. 11, p. 1848, 2018.
[44] President Chure-Tarai Madhesh Conservation Development Board, *Chure Conservation Area (An an Atlas of 36 Districts)*, President Chure-Tarai Madhesh Conservation Development Board, Khumaltar, Lalitpur, Nepal, 2015.
[45] M. S. Thapa and G. Poudel, "Assessing the coverage of urban green space in butwal sub-metropolitan city, Nepal: a gis based approach," *Forestry: Journal of Institute of Forestry, Nepal*, vol. 15, pp. 77–86, 2018.
[46] H. Maas, A. Bienert, S. Scheller, and E. Keane, "Automatic forest inventory parameter determination from terrestrial laser scanner data," *International Journal of Remote Sensing*, vol. 29, no. 5, pp. 1579–1593, 2008.
[47] Askar, N. Nuthammachot, W. Phairuang, P. Wicaksono, and T. Sayektiningsih, "Estimating aboveground biomass on private forest using sentinel-2 imagery," *Journal of Sensors*, vol. 2018, Article ID 6745629, 11 pages, 2018.
[48] J. Chave, M. Réjou-Méchain, A. Búrquez et al., "Improved allometric models to estimate the aboveground biomass of tropical trees," *Global Change Biology*, vol. 20, no. 10, pp. 3177–3190, 2014.
[49] L. S. Khanna and A. N. Chaturvedi, *Forest Mensuration*, Wiley, Hoboken, NJ, USA, 1982.
[50] R. B. Thakur, *A Compendium of Tree Species of Nepal*, Timber Press, Portland, Oregon, 2003.
[51] Ipcc, *Good Practice Guidelines for National Greenhouse Gas Inventories*, IPCC, Geneva, Switzerland, 2006.
[52] A. A. Gitelson and M. N. Merzlyak, "Remote estimation of chlorophyll content in higher plant leaves," *International Journal of Remote Sensing*, vol. 18, no. 12, pp. 2691–2697, 1997.
[53] C. F. Jordan, "Derivation of leaf-area index from quality of light on the forest floor," *Ecology*, vol. 50, no. 4, pp. 663–666, 1969.
[54] J. Delegido, J. Verrelst, L. Alonso, and J. Moreno, "Evaluation of sentinel-2 red-edge bands for empirical estimation of green LAI and chlorophyll content," *Sensors*, vol. 11, no. 7, pp. 7063–7081, 2011.
[55] W. J. Frampton, J. Dash, G. Watmough, and E. J. Milton, "Evaluating the capabilities of Sentinel-2 for quantitative estimation of biophysical variables in vegetation," *ISPRS Journal of Photogrammetry and Remote Sensing*, vol. 82, pp. 83–92, 2013.
[56] J. Peñuelas, I. Filella, P. Lloret, F. Muñoz, and M. Vilajeliu, "Reflectance assessment of mite effects on apple trees," *International Journal of Remote Sensing*, vol. 16, no. 14, pp. 2727–2733, 1995.
[57] A. R. Huete, "A soil-adjusted vegetation index (SAVI)," *Remote Sensing of Environment*, vol. 25, no. 3, pp. 295–309, 1988.
[58] S. K. McFeeters, "The use of the Normalized Difference Water Index (NDWI) in the delineation of open water features," *International Journal of Remote Sensing*, vol. 17, no. 7, pp. 1425–1432, 1996.
[59] N. Puletti, F. Chianucci, and C. Castaldi, "Use of Sentinel-2 for forest classification in Mediterranean environments," *Ann Silvic Res*, vol. 42, pp. 32–38, 2018.
[60] Y. J. Kaufman and D. Tanre, "Atmospherically resistant vegetation index (ARVI) for EOS-MODIS," *IEEE Transactions on Geoscience and Remote Sensing*, vol. 30, no. 2, pp. 261–270, 1992.
[61] A. Huete, C. Justice, and H. Liu, "Development of vegetation and soil indices for MODIS-EOS," *Remote Sensing of Environment*, vol. 49, no. 3, pp. 224–234, 1994.
[62] A. Huete, K. Didan, T. Miura, E. P. Rodriguez, X. Gao, and L. G. Ferreira, "Overview of the radiometric and biophysical performance of the MODIS vegetation indices," *Remote Sensing of Environment*, vol. 83, no. 1-2, pp. 195–213, 2002.
[63] Z. Jiang, A. R. Huete, K. Didan, and T. Miura, "Development of a two-band enhanced vegetation index without a blue band," *Remote Sensing of Environment*, vol. 112, no. 10, pp. 3833–3845, 2008.
[64] Y. Li, M. Li, C. Li, and Z. Liu, "Forest aboveground biomass estimation using Landsat 8 and Sentinel-1A data with machine learning algorithms," *Scientific Reports*, vol. 10, pp. 1–10, 2020.
[65] T. D. Pham, K. Yoshino, and D. T. Bui, "Biomass estimation of Sonneratia caseolaris (l.) Engler at a coastal area of Hai Phong city (Vietnam) using ALOS-2 PALSAR imagery and GIS-based multi-layer perceptron neural networks," *GIScience and Remote Sensing*, vol. 54, no. 3, pp. 329–353, 2017.
[66] N. Nuthammachot, A. Askar, D. Stratoulias, and P. Wicaksono, "Combined use of Sentinel-1 and Sentinel-2 data for improving above-ground biomass estimation," *Geocarto International*, vol. 37, no. 2, pp. 366–376, 2022.
[67] F. F. Muhsoni, A. B. Sambah, M. Mahmudi, and D. G. R. Wiadnya, "Comparison of different vegetation indices for assessing mangrove density using sentinel-2 imagery," *GEOMATE J*, vol. 14, pp. 42–51, 2018.
[68] M. S. Adan, *Integrating Sentinel-2 derived vegetation indices and terrestrial laser scanner to estimate above-ground biomass/ Carbon in Ayer Hitam tropical forest Malaysia*, University of Twente, Enschede, Netherlands, 2017.
[69] A. R. Priatama, Y. Setiawan, I. Mansur, and M. Masyhuri, "Regression models for estimating aboveground biomass and stand volume using landsat-based indices in post-mining area," *Jurnal Manajemen Hutan Tropika (Journal of Tropical Forest Management)*, vol. 28, pp. 1–14, 2022.
[70] A. Fernández-Manso, O. Fernández-Manso, and C. Quintano, "SENTINEL-2A red-edge spectral indices suitability for discriminating burn severity," *International Journal of Applied*

Earth Observation and Geoinformation, vol. 50, pp. 170–175, 2016.

[71] B.-B. Guo, S.-L. Qi, Y.-R. Heng et al., "Remotely assessing leaf N uptake in winter wheat based on canopy hyperspectral red-edge absorption," *European Journal of Agronomy*, vol. 82, pp. 113–124, 2017.

[72] F. M. Padilla, M. T. Peña-Fleitas, M. Gallardo, and R. B. Thompson, "Determination of sufficiency values of canopy reflectance vegetation indices for maximum growth and yield of cucumber," *European Journal of Agronomy*, vol. 84, pp. 1–15, 2017.

[73] C. Wang, M.-C. Feng, W.-D. Yang et al., "Impact of spectral saturation on leaf area index and aboveground biomass estimation of winter wheat," *Spectroscopy Letters*, vol. 49, no. 4, pp. 241–248, 2016.

[74] O. Mutanga and A. K. Skidmore, "Hyperspectral band depth analysis for a better estimation of grass biomass (Cenchrus ciliaris) measured under controlled laboratory conditions," *International Journal of Applied Earth Observation and Geoinformation*, vol. 5, no. 2, pp. 87–96, 2004.

[75] D. Lu, Q. Chen, G. Wang, L. Liu, G. Li, and E. Moran, "A survey of remote sensing-based aboveground biomass estimation methods in forest ecosystems," *International Journal of Digital Earth*, vol. 9, no. 1, pp. 63–105, 2016.

[76] S. Das and T. P. Singh, "Correlation analysis between biomass and spectral vegetation indices of forest ecosystem," *International Journal of Engineering Research and Technology*, vol. 1, pp. 1–13, 2012.

[77] S. Sinha, C. Jeganathan, L. K. Sharma, M. S. Nathawat, A. K. Das, and S. Mohan, "Developing synergy regression models with space-borne ALOS PALSAR and Landsat TM sensors for retrieving tropical forest biomass," *Journal of Earth System Science*, vol. 125, no. 4, pp. 725–735, 2016.

[78] I. K. Wernick, P. Ciais, J. Fridman et al., "Quantifying forest change in the European Union," *Nature*, vol. 592, no. 7856, pp. E13–E14, 2021.

[79] D. Lu, Q. Chen, G. Wang et al., "Aboveground forest biomass estimation with Landsat and LiDAR data and uncertainty analysis of the estimates," *International Journal of Financial Research*, vol. 2012, Article ID 436537, 16 pages, 2012.

[80] M. K. Steininger, "Satellite estimation of tropical secondary forest above-ground biomass: data from Brazil and Bolivia," *International Journal of Remote Sensing*, vol. 21, no. 6-7, pp. 1139–1157, 2000.

[81] DFRS, *Churiya Forest of Nepal*, Forest Resource Assessment Nepal Project, Babarmahal, Kathmandu, Nepal, 2014.

[82] N. Badreldin and A. Sanchez-Azofeifa, "Estimating forest biomass dynamics by integrating multi-temporal Landsat satellite images with ground and airborne LiDAR data in the Coal Valley Mine, Alberta, Canada," *Remote Sensing*, vol. 7, no. 3, pp. 2832–2849, 2015.

[83] O. A. Macave, N. S. Ribeiro, A. I. Ribeiro et al., "Modelling aboveground biomass of miombo woodlands in niassa special reserve, northern Mozambique," *Forests*, vol. 13, no. 2, pp. 311–316, 2022.

[84] F. E. Fassnacht, F. Hartig, H. Latifi et al., "Importance of sample size, data type and prediction method for remote sensing-based estimations of aboveground forest biomass," *Remote Sensing of Environment*, vol. 154, pp. 102–114, 2014.

[85] S. Vafaei, J. Soosani, K. Adeli et al., "Improving accuracy estimation of Forest Aboveground Biomass based on incorporation of ALOS-2 PALSAR-2 and Sentinel-2A imagery and machine learning: a case study of the Hyrcanian forest area (Iran)," *Remote Sensing*, vol. 10, no. 2, p. 172, 2018.

[86] G. Ou, C. Li, Y. Lv et al., "Improving aboveground biomass estimation of Pinus densata forests in Yunnan using Landsat 8 imagery by incorporating age dummy variable and method comparison," *Remote Sensing*, vol. 11, no. 7, p. 738, 2019.

[87] D. Morin, M. Planells, D. Guyon et al., "Estimation and mapping of forest structure parameters from open access satellite images: development of a generic method with a study case on coniferous plantation," *Remote Sensing*, vol. 11, p. 1275, 2019.